ARTICLE

Precipitation of Silver Particles with Controlled Morphologies from Aqueous Solutions

Received 00th January 20xx,
Accepted 00th January 20xx

DOI: 10.1039/x0xx00000x

Lijuan Wang, [a] Jens-Petter Andreassen [a] and Seniz Ucar *[a]

Synthesis of silver particles with controlled morphologies enables their use in a variety of applications. Although several synthetic approaches have been developed to successfully modify the final particle shape, the underlying mechanism controlling the shape development is yet under extensive debate including the so-called classical and nonclassical theories of crystal growth. Here we explore the variation of silver morphologies as a function of reactant concentrations and pH, during reduction of silver nitrate with ascorbic acid in aqueous solutions. It was shown that enhancing the redox potential in solution via increasing the reductant concentration resulted in a stepwise change in morphology from polyhedral to hopper and dendritic particles, whereas the reverse order was observed when the redox reaction was repressed by decreasing the solution pH. Spherulites were obtained under very high driving force that was satisfied via either high precursor concentrations or high pH. Our results demonstrate the strong correlation of particle morphology with solution supersaturation, which was elucidated within the framework of crystallographic and non-crystallographic branching mechanisms for the formation of dendrites and polycrystalline spherulites, respectively.

Introduction

Synthesis of crystalline silver particles with diverse morphologies in both nano- and micro-scale has received increased attention in recent years due to their unique properties and important potential applications in various fields, such as catalysis[1], silicon solar cells[2], surface enhanced Raman spectroscopy[3], self-cleaning films[4], and antibacterial materials.[5] For many of these applications, morphology control has been pivotal due to its strong implications on the characteristics of the silver particles. Several synthetic approaches have been developed to successfully modify the final particle shape, however, the underlying mechanism controlling the shape development is yet to be fully understood.[6]

Controlling the morphology of crystalline particles requires a clear understanding of the fundamental growth mechanism. Currently, the so-called classical and non-classical concepts of crystal growth coexists in literature to explain the formation of mono- and polycrystalline particles, and complex morphologies.[7] In the classical picture, crystals grow by continuous addition of monomeric growth units from the solution to the solid crystal lattice, and the thermodynamic driving force, i.e. supersaturation, determines the growth mechanism with implications on final morphology. The non-classical theories have emerged to explain the formation of crystalline particles with nanosized surface features and complex morphologies, and typically attribute the size enlargement of the particles to aggregation or assembly of nano-sized primary crystals.[8]

Numerous studies have been performed on the production of crystalline silver particles by reducing silver ions to their elemental state, and both classical and nonclassical crystal growth mechanisms have been proposed to explain their formation. One of the early attempts on a nonclassical interpretation is the well-known nano-aggregation mechanism which was proposed by Matijević as the underlying mechanism for various monodispersed mineral colloids due to the observation of their spherical shape and polycrystallinity.[9, 10] This mechanism was explained by initial formation of irregular nano-sized primary particles due to diffusional growth of crystal nuclei and then their aggregation to form final secondary large particles, and has been frequently used to explain the formation of polycrystalline, spherical silver particles in the literature.[2, 11-16] Later, Penn and Banfield proposed the oriented attachment mechanism as an alternative enlargement path for nano-sized crystals, where the adjacent particles share a common crystallographic orientation by spontaneous self-organization and assemble together in a planar interface.[17, 18] The driving force for this process is to decrease the overall free energy by eliminating the surface energy relevant to the unsatisfied bonds between these particles. It is proposed that when the oriented attachment is not perfect, dislocations generate even though the initial nuclei are defect-free.[19] For silver particles, previous work suggested that spherulites were formed by random nano-

[a] Department of Chemical Engineering, Norwegian University of Science and Technology, Trondheim, Norway

Electronic Supplementary Information (ESI) available: [SEM images of silver particles precipitated in experimental series 2 and 4, solution speciation of series 3 calculated by Visual Minteq thermodynamic software]. See DOI: 10.1039/x0xx00000x

aggregation, while dendrites and sheet-like[1], rosette-like[3], polyhedral[4], flower-like[20], and 3D flower-like superstructures[21] were formed by oriented attachment of minute primary particles. Stimulated by Forrest and Witten's work, which demonstrated the formation of fractal aggregates of small metal particles in dense gas, Witten and Sander introduced the diffusion-limited aggregation (DLA) model in 1981.[22, 23] The DLA model is a computer simulation model describing how particles are added from long-range distance, one at a time, to the growing cluster through random pathways, and finally stick together to form fractal aggregates. Lately, several studies have used this model to explain the formation of silver dendrites by proposing that small silver particles/clusters were formed first, and then diffused to the growing structure and stuck together when they contacted each other to form silver dendritic particles.[24-28] Mesocrystals, which was proposed by Cölfen *et al.* in the field of biomineralization[29], were defined as highly ordered superstructures of nanoparticles for both monocrystallline and polycrystalline materials. Their proposed formation pathway includes nano-sized primary particles that go through mesoscale assembly with crystallographic co-orientation to produce mesocrystals[30]. Fang *et al.* proposed this mechanism for the formation of a variety of silver crystal morphologies, such as plate-like structures[31], dendrites[32], spherulites[33], mesocages[34] and mesocubes[35] by either aqueous crystallization or a sacrificial template method.

Meanwhile, same observations that led to the non-classical hypotheses are elucidated within the classical models by extending the fundamental approach of classical theory to explain the formation of dendritic and spherulitic morphologies along with polyhedral crystals. According to the classical theory of crystal growth, by adjusting the level of the crystallization driving force (supersaturation), different growth mechanisms can be evoked, as a result of which the particle morphologies change from polyhedral to hopper, dendritic and spherulitic particles, as shown schematically in Figure 1.[36] At low to moderate supersaturation levels, growth is controlled by the incorporation of monomers into the crystal lattice by surface reactions that results in polyhedral crystals with smooth faces.[37] At high levels of supersaturation, the monomer integration rate increases with extensive surface nucleation and the growth mode changes from an integration-controlled to a diffusion-controlled mechanism. Inhomogeneities in the diffusion field around the crystal and differences in the relative growth rates of individual crystal faces result in formation of hopper crystals, and further crystallographic branching that forms dendrites. Previous work on silver particles synthesized via solution-based chemical reduction and electrochemical processes showed shifting morphologies from polyhedrals to dendrites with the corresponding changes in the growth regime.[38, 39] It has been well-documented that the anisotropic interfacial properties and inhomogeneous diffusion fields around the crystals lead to dendritic growth.[40-42] Haxhimali *et al.* demonstrated both computationally and experimentally that the range of possible dendrite growth directions can vary continuously between different crystallographic directions as a function of the composition-dependent anisotropy parameters such as interfacial energy and stiffness of the crystal faces, and clarified the richer morphological diversity of the resulting dendritic structures than previously anticipated.[43] At yet higher supersaturation levels, surface nucleation at the growth front is no longer crystallographic, which means the freshly formed sub-individuals show different lattice orientations with respect to the parent branch, as compared to the crystallographic branching of dendrites. The subsequent polycrystalline structure is a result of the accumulated internal stress under very high driving force and its release by misoriented growth front nucleation (GFN). By the orientation-field-based phase-field models, Gránásy *et al.* simulated two types of spherulite formation as type 1 and type 2, where spherulites form either through a central multidirectional growth or via a unidirectional growth with low angle branching, respectively.[44, 45] They also demonstrated the morphology change from single needle crystals to polycrystalline spherulites with increasing supersaturation with phase-field modeling.[46] These theoretical predictions have been supported by experimental observations of spherulite formation via the suggested non-crystallographic branching mechanisms.[47-49] Although spherulitic growth was first noticed by investigations of crystallization from viscous melts and polymers; molecular, atomic and ionic crystals can all grow spherulite particles.[49, 50] In solution crystallization, neither high viscosity nor specific additives are prerequisite to spherulitic growth, but high driving force for crystallization is.[50, 51] The work of Shtukenberg *et al.* provides a comprehensive review on the growth of spherulites for interested readers.[50]

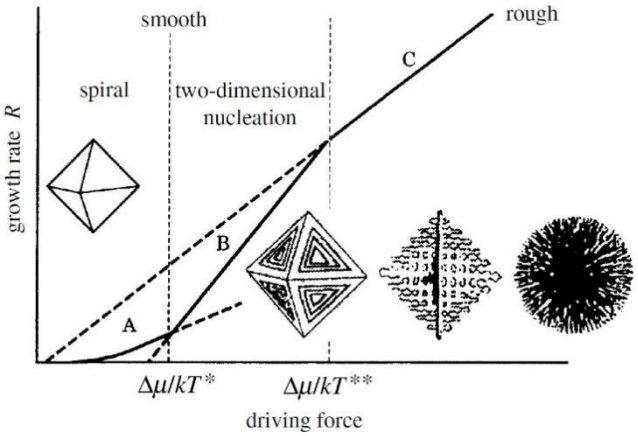

Figure 1. Morphology change of crystalline particles as a function of the driving force, i.e. supersaturation, according to classical crystal growth theory.[36] At low to moderate driving force, reaction-controlled growth mechanisms result in monocrystalline polyhedral crystals with smooth faces. At high driving force, growth mechanism is diffusion-controlled and depending on the level of supersaturation crystallographic and noncrystallographic branching occur that result in dendrites and polycrystalline spherulites, respectively. Figure is adapted from reference 36 with permission.

In the present study, we aim to explore the mechanism behind the formation of a diversity of silver morphologies. The two size enlargement mechanisms that coexist in literature are originated from different fundamental backgrounds and consequently rely on different process parameters. Thus, systematic studies of reaction parameters can help us gain insight on the acting growth mechanisms. In this work, silver particles were precipitated by reduction of silver nitrate with ascorbic acid in aqueous solutions without additives. A complete series of morphologies were obtained, from polyhedral crystals to spherulites, by regulating the reaction conditions via reactant concentrations and pH. Here we show that the morphological variations can be explained with the different supersaturation profiles generated at each experimental condition that evoke different growth mechanisms.

Experimental

Silver nitrate ($AgNO_3$) (≥ 99%), ascorbic acid (AA) and ammonia (NH_3, 25%, aq.) were purchased from Sigma-Aldrich. Nitric acid solution (HNO_3, 65%) was from Merck. Deionized water was used to prepare all aqueous solutions. Both ammonia and nitric acid were used directly without any dilution for controlling the pH conditions in the solution.

All experiments were carried out in a 100 mL glass reactor with a lid having two baffles attached. The reactor was jacketed for temperature control (25.0 ± 0.2 ºC) and stirred by a magnetic stirrer with digital display (1200 rpm). Equal volumes (50 mL each) of silver nitrate ($AgNO_3$) and ascorbic acid solutions (AA) were mixed at different concentrations as explained in Table 1. For experiments with large volumes of nitric acid or ammonia addition (5 mL and more), the dilution effect was considered by decreasing the water content in both the $AgNO_3$ and AA solutions accordingly. The chemical speciation in solutions after mixing was determined by the thermodynamic calculation program PHREEQC Interactive 3.1 (U.S. Geological Survey, Reston, VA, USA), using the Minteq v4 database, assuming the conditions prior to reduction in solution. For the calculations, the pH and temperature of the solution and the concentrations of constituent ions were provided as input data. The solution speciation is then calculated by the software by taking into account all possible reactions in solution.

Table 1. Reactant compositions at different experimental conditions

Experiment series	*$AgNO_3$/AA concentration (mM)*	*V_{HNO3} added (mL)*	*V_{NH3} added (mL)*
1	10/5, 10/20, 10/50, 10/70, 10/100	1, 0.2	-
2	10/50	0 ~ 2	0.05 ~ 0.8
3	20/100	0 ~ 10	0.05 ~ 1
4	200/1000	0 ~ 2	0.05 ~ 10

In a typical precipitation run, AA solution was added into the reactor first, and then controlled amounts of HNO_3 (65%) or NH_3 (25%, aq.) solutions were added to adjust the pH (see Table 1), and the pH values were recorded by a Mettler-Toledo SevenEasy pH meter (Figure S1). Next, the $AgNO_3$ solution was added rapidly into the strongly agitated AA solution. After mixing the reactants, a short induction period occurred during which there was a sharp change of the solution color from transparent to milk white, grey white, dark grey or brown, depending on the different experimental conditions. The induction time was measured manually by a stopwatch and three parallels for each experimental condition were performed. All experiments were kept running for 5 minutes, and the resulting silver particles were separated by filtering with a 0.22 μm Millipore filter membrane and washed with deionized water and ethanol prior to drying at 60 ˚C. In order to examine the effect of ammonia on the silver precipitation, replicate experiments were conducted by adjusting the pH of the AA solution at pH 10 either with ammonia (25%, aq.) or sodium hydroxide (0.1 M) solution, at an $AgNO_3$/AA = 0.1/0.5 mM concentration by using the same procedure as described above.

Morphology of silver particles was examined using scanning electron microscopy (SEM) (S-5500, Hitachi, Japan) images of dried powder samples at an accelerating voltage of 15-30 kV. Particle size was analyzed by counting approximately 200 ~ 300 particles for each parallel from the SEM images. Transmission electron microscopy (TEM) was performed using a JEOL JEM 2100 microscope fitted with a LaB6 cathode (JEOL, 8 Tokyo, Japan) at an accelerating voltage of 200 kV. Thin cross sections of samples for TEM were prepared as follows: powder samples were mixed with epoxy resin and cured at 60 °C for three days. Thin sections (80 nm) were cut from the resin block using a microtome (Ultracut S, Reichert, USA) equipped with a diamond knife (ultra 45°, DiATOME, USA) and placed on Cu grids with a lacey carbon film (300 mesh, Agar Scientific, UK). Diffraction patterns were analyzed using DiffTools in Digital Micrograph software (version 3.31, Gatan). Characterization of solid phases were conducted via powder X-ray Diffraction (XRD) (D8 Advance, Bruker AXS GmBH, Karlsruhe, Germany) in the 2θ range of 20-80°with a step size of 0.013°.

Results and discussion

Varying the molar ratio of $AgNO_3$/AA at fixed acidic conditions

In experiment series 1, the concentration of AA was varied in the reaction medium while $AgNO_3$ concentration and the volume of nitric acid were kept constant (Table 1). The pH of the AA solutions was adjusted to 0.7 or 1.5 before the addition of silver precursor. Since both pH values are below the first dissociation constant of AA, pKa_1 = 4.04, the reductant was dominantly present in its fully protonated form, H_2A (Figure S2). The reactivity of silver precursor depends on its speciation in solution, i.e. free concentration of silver ions and formation of ion pairs, thus, is a function of the pH of the reaction medium. In addition, the electrode potentials of both silver and ascorbic

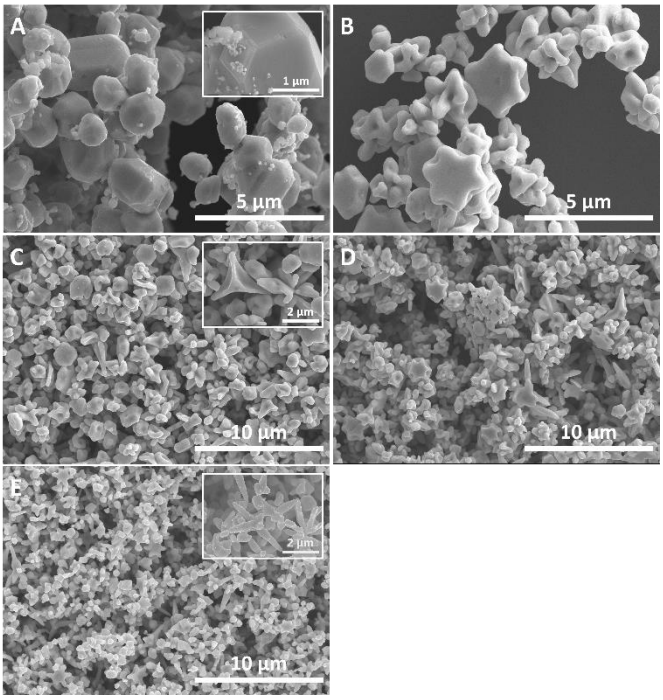

Figure 2. SEM image of silver particles formed at pH 0.7 with different molar ratios of $AgNO_3$/AA (mM/mM): (A) 10/5, (B) 10/20, (C) 10/50, (D) 10/70 and (E) 10/100.

acid precursors vary with pH.[52] Thus, maintaining a constant initial pH ensured that AA concentration was the dominating reaction parameter in this data set.

SEM images of the final precipitates showed that at conditions of 1:0.5 molar ratio, faceted polyhedral particles were obtained at both initial pH values (Figure 2A and 3A). At pH 0.7, when the molar ratio of AA was increased to 1:2 and 1:5 with respect to silver concentration, hopper crystals and the onset of dendritic growth was observed, respectively (Figure 2B and 2C). Further increasing the concentration of the reducing agent did not evoke a purely mass transfer-controlled growth or dendritic/spherulitic particles at this pH, but rather reduced particle size with similar morphologies (Figure 2D and 2E). On the other hand, at pH 1.5, increasing the AA concentration at a ratio of 1:5 and 1:10 resulted in formation of dendrites and spherulites, respectively (Figure 3B and 3C).

In an aqueous solution, the activity-based supersaturation for silver is defined as the ratio of the activity of atomic silver in solution to its equilibrium value at a constant temperature. The activity and the generation rate of the atomic silver determines the supersaturation profile in the reaction medium and depends on the electrode potential and kinetics of the redox reaction. In the acidic medium, the overall redox reaction proceeds with either one-electron or two-electrons oxidation of ascorbic acid, as given in Equation 1 and 2, respectively (see supplementary information section B):

$$Ag^+ + H_2A \rightarrow Ag^0 + A^{\cdot -} + 2H^+ \qquad \text{(Eq. 1)}$$

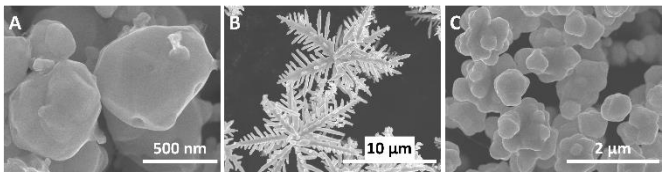

Figure 3. SEM image of silver particles formed at pH 1.5 with different molar ratios of $AgNO_3$/AA (mM/mM): (A) 10/5, (B) 10/50, (C) 10/100.

$$2Ag^+ + H_2A \rightarrow 2Ag^0 + A + 2H^+ \qquad \text{(Eq. 2)}$$

Increasing the concentration of the reducing agent leads to enhanced redox kinetics and increases the generation rate of silver atoms as can be deduced from Equations 1 and 2.[53] Consequently, supersaturation can build up to higher levels and invoke a mass-transfer controlled growth mechanism as a result of extensive surface nucleation and fast integration kinetics. Thus, the diffusion field around crystals becomes prominent on their development and certain faces of the crystals can have higher relative growth rates.[7] The stepwise change of morphology from polyhedral to hopper particles followed by dendritic onset and branched morphologies demonstrated this gradual change in the growth mode with increasing driving force for crystallization. In addition, the decrease in particle size with similar morphologies at pH 0.7 (Figure 2D and 2E) further confirmed that supersaturation was escalating in the reaction medium with increasing AA concentration, since nucleation rate increases exponentially with supersaturation and yields higher number of nuclei that consume the remaining supersaturation for growth.[54]

Similar structural changes were reported in literature also when the thermodynamic driving force for growth was augmented by increasing the concentration of the silver precursor, and the resulting shift from polyhedral to dendritic forms were similarly explained by the change in growth regime towards a diffusion-controlled mechanism.[55-57] In addition, Liu *et al.* demonstrated a reversible transition between compact morphologies and dendrites of silver by decreasing or increasing the reduction rate of silver, respectively.[58] Yang *et al.* and Liu *et al.* showed that the morphology of silver particles can be altered from polyhedral to dendritic structures also by modifying the solvent viscosity via introduction of glycerol in the reaction medium to induce a concentration gradient in the system.[39, 59] They attributed the variations in particle morphology to the changing diffusion field around the crystals and explained the formation of fractal structures by the resulting instability near the growth front. These studies show the dependence of the final particle morphology on the growth mechanism in action, which can be controlled via modifying the thermodynamic driving force and the reaction kinetics. Other studies showed a similar morphology change by increasing the reductant concentration in solution, and alternatively attributed this behavior to a diffusion-limited aggregation (DLA) mechanism.[28, 60] However, this suggestion is mainly based on final morphology observations in these cases that do not reveal what processes

led to the crystal formation. In a recent study, Liu *et al.* confirmed the dependence of the particle branching on thermodynamic driving force and anisotropic growth kinetics for zinc oxide nanoparticles by real time monitoring of their formation via in-situ liquid phase scanning electron microscopy and by coupling these observations with high-resolution transmission electron microscopy in combination with classical density functional theory, they reported that neither random aggregation nor oriented attachment was observed.[61]
These results clearly demonstrated the dependence of growth mechanism on the supersaturation build up in the solution, which can be regulated by the precursor concentrations. Moreover, it was shown that pH was also a parameter that determines the range of attainable silver morphologies. Therefore, its role was investigated in detail in the following experimental sets.

Varying the pH at a fixed molar ratio of $AgNO_3$/AA

In order to study the full range of particle morphologies, the initial supersaturation must be tuned to allow for different growth modes. For this purpose, the pH of the system was also varied to manipulate the redox reaction and thus the supersaturation, as well as the reactant concentrations at a fixed molar ratio of $AgNO_3$/AA = 1:5 (series 2, 3 and 4 in Table 1).

Since it was not possible to quantify the supersaturation in our experimental setup, induction time was used as an indicator of initial solution supersaturation at varying experimental conditions (Figure 4). It was observed that at similar pH values increasing the reactant concentrations reduced the induction time, as expected, due to increasing initial supersaturation. Data also showed shorter induction times with increasing pH for series 2 and 3, whereas for series 4 the effect of pH became indistinct.

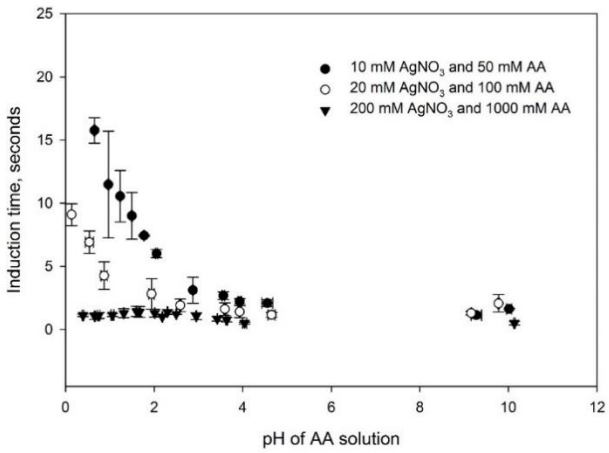

Figure 4. Induction time as a function of the initial pH of AA solution at three different reactant concentration levels with a fixed molar ratio of $AgNO_3$/AA = 1:5.

Among the three experimental sets, in series 3 with the concentration of $AgNO_3$/AA = 20/100 mM all morphologies from polyhedral particles to spherulites were observed with hopper and dendritic intermediate steps via the gradual variation of the pH of AA solution from -0.19 to 9.78 (Figure 5). The stepwise changes in morphology and induction times were in good correlation to point towards an increasing driving force for crystallization with increasing pH. Same trends were observed in series 2 also, however, although the precursor concentrations were lower compared to series 3, polyhedral crystals were not obtained in this data set (Figure S3). The lowest pH in series 2 was 0.65 and this showed the deterministic role of pH on the growth mechanism and the final crystal morphology. In series 4, the precursor concentrations were very high, resulting in a high driving force and a diffusion-limited growth regime under all pH conditions in the range of 0.39 to 10.13, thus, only dendrites and spherulites were observed (Figure S4).

In series 3 without any pH adjustment (pH_{AA}= 2.59), the crystals attained spherulitic morphologies, showing that the driving force during growth was high enough in the system to result in non-crystallographic branching due to high concentrations of the precursors (Figure 5E). As the pH of the medium was lowered by the addition of nitric acid; dendritic, hopper and polyhedral crystals were observed, respectively (Figure 5C to 5A). Although the oxidation potential of AA slightly decreases with increasing pH, at acidic conditions, lower pH shifts the reaction equilibrium towards the reactants in accordance with the Le Chatelier's principle (Equations 1 and 2). In addition, previous work showed that the reduction rate of AA increases with pH in the acidic range, i.e. with the prevalence of the deprotonated form, HA^-.[62, 63] In their study, Yang *et al.* quantitatively showed the reduced reaction rate for the same system with increasing amounts of acid in the medium, accordingly.[38] Moreover, lower pH values require high acid concentration in the reaction medium and the thermodynamic calculations showed that, activity of silver ions in solution was decreasing with increasing amounts of nitric acid due to [$AgNO_3$] complexation (Figure S5). Thus, we conclude that lowering the pH interferes with the supersaturation build-up in the reaction medium, which consequently results in a shift towards a reaction-controlled growth regime and formation of monocrystalline equilibrium morphologies.[36, 51]

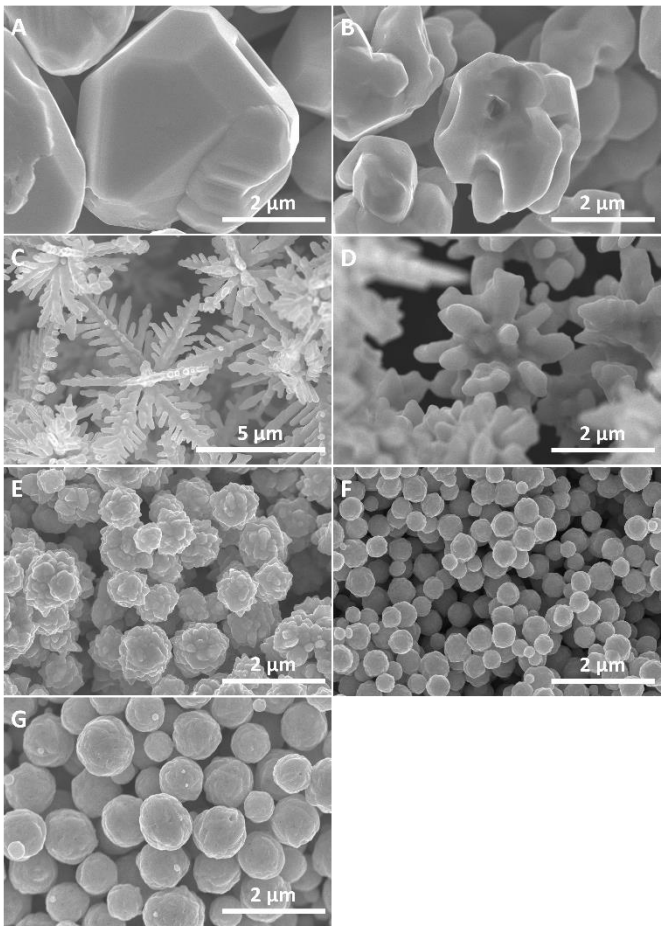

Figure 5. SEM image of silver particles formed at $AgNO_3$/AA = 20 mM/100 mM (experiment series 3), where initial pH of the AA solution was varied at: (A) -0.19, (B) 0.14, (C) 1.39, (D) 1.94, (E) 2.59, (F) 9.16, and (G) 9.78.

The changes in the particle crystallinity with the acting growth mechanism as a function of the supersaturation level were demonstrated by the electron diffraction data collected from the thin cross sections of polyhedral and spherulite samples (Figure 6). Polyhedral crystals obtained at low driving force were shown to be monocrystalline, whereas spherulites that form as a result of non-crystallographic branching at high supersaturation showed diffraction rings corresponding to their polycrystalline nature.

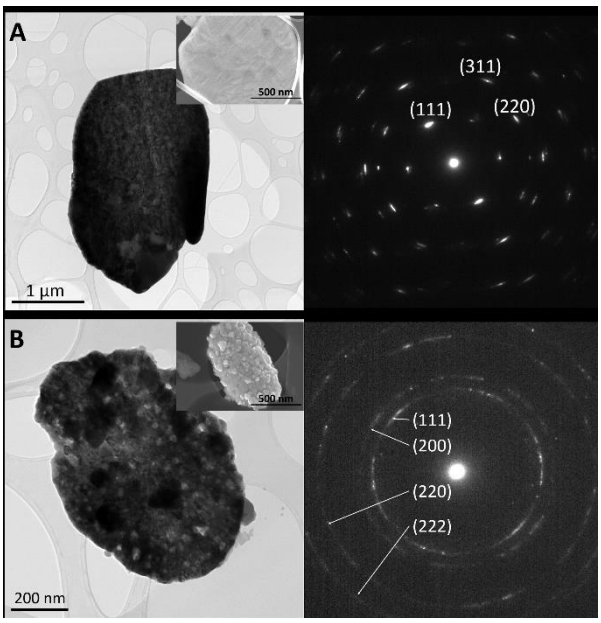

Figure 6. TEM images and electron diffraction patterns of the thin cross-sections of a (A) polyhedral and (B) spherulitic particle. Insets show the SEM images of the cross-sections for each particle.

The transition trends from dendrites to spherulites were similar for all series. While decreasing the pH led to less sub-branched dendrites to hopper particles, increasing the pH resulted in shorter dendritic branches and a change towards radial outgrowing plate-like structures and spikes, as shown in Figure 5D, S3C and S4C. These plate-like structures and spikes were also observed in gold and calcium carbonate particles and interpreted as a transition from monocrystalline to polycrystalline growth region with increasing driving force for crystallization.[64, 65] When pH was further increased, these plate-like structures and spikes became shorter (Figure 5E, S3D and S4D), and finally spherulites were formed (Figure 5F, S3E and S4E). Spherulitic growth was observed as a result of high rates of growth front nucleation (GFN) with higher supersaturation attained at high pH. This observation is in accordance with the phase field modeling results by Gránásy *et al.* that show spherulite formation with more space-filling patterns as a result of increased supersaturation and GFN rates.[44] At basic pH, fully formed closed spherulites are observed in all series (Figure 5F and 5G, S3E and S3F, S4E and S4F).

High pH in the reaction media was achieved via addition of ammonia to the AA solution. Under the corresponding conditions, silver ions form complexes with ammonia, and the solution speciation is gradually dominated by $[Ag(NH_3)_2]^+$, which is then reduced. The standard reduction potential of $[Ag(NH_3)_2]^+/Ag$ (0.373 V) is lower than that of Ag^+/Ag (0.799 V).[53] In addition, deprotonation of ascorbic acid at high pH results in formation of ascorbate mono- and dianion, which have lower oxidation potentials compared to AA.[66] Yet, formation of spherulites indicated a high driving force for crystallization in the system, which is attributed to the effect of pH on the

reaction kinetics of the oxidation half reaction where increasing pH leads to faster redox kinetics and an efficient supersaturation build-up. These results coincide with the work of Williams *et al.*, which showed that the rate constants for the oxidation of ascorbate anions increase significantly with increasing pH.[67]

Previous studies of silver reduction with AA also showed spherulite formation at basic pH, and reported increasing particle size with increasing ammonia concentration.[16, 68, 69] We also observed a similar trend where the average diameter of spherulites increased from 403 nm to 770 nm (Figure 5F and 5G) and from 490 nm to 630 nm (Figure S3E and S3F) with increasing ammonia content. Larger particle sizes were ascribed to higher nucleation and aggregation rates within the framework of particle-based growth hypotheses. However, in the classical picture, increasing particle size is often a result of lower nucleation rates that indicate a lower initial supersaturation.

The complex role of ammonia addition to the system leads to contradictory effects on the electrode potential and the kinetics of the redox reaction, which synergistically affect the supersaturation file in the reaction medium. Addition of ammonia increases the solution pH and induce faster redox kinetics. On the other hand, complexation of silver ions lowers the redox potential. In order to decouple the effects of high pH and ammonia presence in the reaction medium, we conducted supplementary experiments, where solution pH was adjusted to ≈10.0 with either NH_3 or NaOH, at constant precursor concentrations (for further information on pH variation with NaOH, see supplementary information Figure S6). The solution speciation of silver species at each experimental condition was estimated by thermodynamic calculations and showed that 99 % of silver was found as $[Ag(NH_3)_2]^+$ in the presence of NH_3, while only 10% of silver formed complexes with hydroxide ions in the presence of NaOH (Figure 7A). At constant pH and concentration, large polyhedral particles were observed in the presence of NH_3, whereas, the precipitates showed the onset of spherulites in the presence of NaOH (Figure 7). These results clearly demonstrated the inhibiting effect of ammonia complexation on the supersaturation build up. Therefore, we propose that, in our experiments high pH promoted the spherulite formation by augmenting the initial supersaturation development, however, further increasing the ammonia content induced an opposite effect on supersaturation that in turn resulted in larger particles.

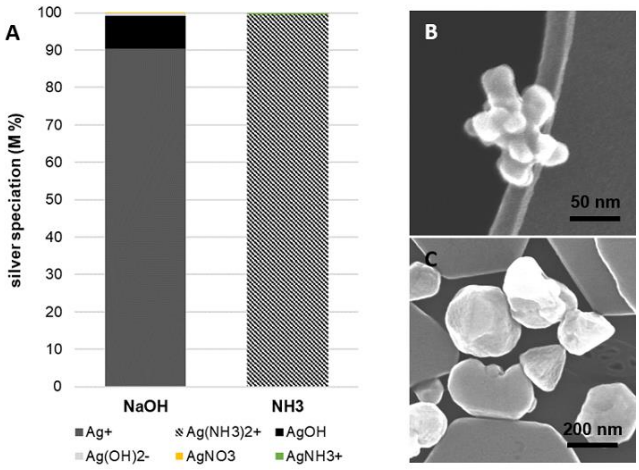

Figure 7. (A) Percent distribution of total concentration of silver species assuming the conditions prior to reduction in solution with the indicated bases used to adjust the pH at 10, at the precursor concentrations of $AgNO_3$/AA = 0.1 mM/0.5 mM, and the SEM images of final silver particles formed in the presence of (B) NaOH, and (C) NH_3.

Characterization of the final precipitates by XRD showed the prominent diffraction peaks of crystalline silver for all morphologies observed in series 3 (Figure 8). The polyhedral and dendritic particles (shown in Figure 5A and 5C) displayed narrow diffraction peaks, indicating their high crystallinity, whereas spherulitic particles (shown in Figure 5E) showed a slight peak broadening. Relatively broad XRD peaks observed in spherulites have been used to support aggregation mechanisms and to calculate the size of alleged primary particles by the Scherrer equation.[70-72] However, by investigating calcite crystals co-precipitated with polymers, Kim *et al*. have proved that the peak broadening occurs due to lattice strain only, and provides no evidence for a nano-aggregation mechanism.[73] On the other hand, observation of peak broadening due to lattice strain hints on the internal stress of spherulites that drives non-crystallographic branching for relaxation.[50, 74]

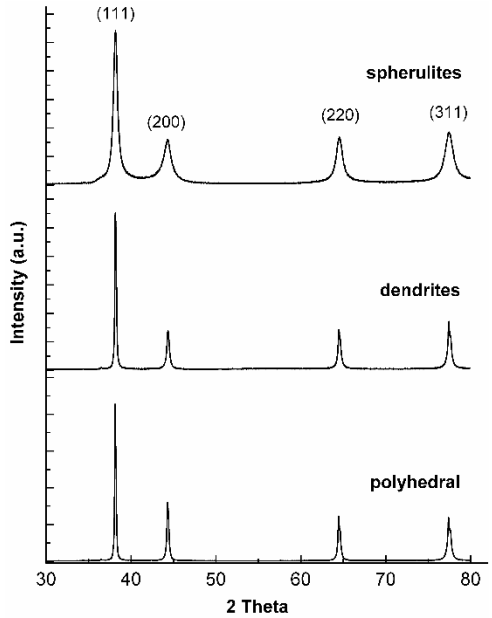

Figure 8. XRD patterns of spherulites, dendrites and polyhedral particles showing the prominent diffraction peaks of crystalline silver.

Conclusions

Synthesis of silver particles with controlled morphologies can be achieved when the underlying growth mechanisms and the parameters that control growth are identified. In this work, we showed that by regulating the pH and reactant concentrations, silver particles with a variety of morphologies can be fabricated as a result of effective control on the supersaturation profiles. It was shown that the redox kinetics that is responsible for the generation of atomic silver, i.e. supersaturation in the system, can be enhanced by increasing the concentrations of the silver precursor and the reducing agent, as well as by increasing the pH. Stepwise changes in the driving force for crystallization towards higher values, resulted in a gradual change of particle morphologies from polyhedral to spherulitic particles with hopper and dendritic intermediate morphologies. This dependence demonstrated the decisive role of supersaturation on the acting growth mechanism and its implications on the particle morphology. In accordance, crystallographic and non-crystallographic branching mechanisms were suggested for the formation of dendrites and spherulites, respectively. The results of this study can be used to further fine tune the silver morphologies for shape selective applications.

Conflicts of interest

There are no conflicts to declare.

Acknowledgements

The authors would like to thank Ragnhild Sæterli for her assistance with the TEM sample preparation and analyses. The Research Council of Norway is acknowledged for the support to the Norwegian Micro and Nanofabrication Facility, NorFab, project number 245963/F50.

References

1. G. Yuan, X. Chang and G. Zhu, *Particuology*, 2011, **9**, 644-649.
2. Z. Liu, X. Qi and H. Wang, *Advanced Powder Technology*, 2012, **23**, 250-255.
3. M. F. Zhang, A. W. Zhao, H. Y. Guo, D. P. Wang, Z. B. Gan, H. H. Sun, D. Li and M. Li, *Crystengcomm*, 2011, **13**, 5709-5717.
4. C. Gu and T.-Y. Zhang, *Langmuir*, 2008, **24**, 12010-12016.
5. X. Chen and H. J. Schluesener, *Toxicology Letters*, 2008, **176**, 1-12.
6. T. Liu, W. Liu, Y. Chen, T. Yang and Y. Han, *Chemical Engineering and Processing - Process Intensification*, 2018, **134**, 38-44.
7. J.-P. Andreassen and A. E. Lewis, in *New Perspectives on Mineral Nucleation and Growth: From Solution Precursors to Solid Materials*, eds. A. E. S. Van Driessche, M. Kellermeier, L. G. Benning and D. Gebauer, Springer International Publishing, Cham, 2017, DOI: 10.1007/978-3-319-45669-0_7, pp. 137-154.
8. J. J. De Yoreo, P. U. P. A. Gilbert, N. A. J. M. Sommerdijk, R. L. Penn, S. Whitelam, D. Joester, H. Zhang, J. D. Rimer, A. Navrotsky, J. F. Banfield, A. F. Wallace, F. M. Michel, F. C. Meldrum, H. Cölfen and P. M. Dove, *Science*, 2015, **349**.
9. E. Matijevic, *Chem Mater*, 1993, **5**, 412-426.
10. E. Matijević, *Colloid J+*, 2007, **69**, 29-38.
11. K. P. Velikov, G. E. Zegers and A. van Blaaderen, *Langmuir*, 2003, **19**, 1384-1389.
12. L. Suber, I. Sondi, E. Matijevic and D. V. Goia, *Journal of Colloid and Interface Science*, 2005, **288**, 489-495.
13. D. T. Robb, I. Halaciuga, V. Privman and D. V. Goia, *J Chem Phys*, 2008, **129**.
14. I. Halaciuga and D. V. Goia, *J Mater Res*, 2008, **23**, 1776-1784.
15. B. An, X.-h. Cai, F.-s. Wu and Y.-p. Wu, *Transactions of Nonferrous Metals Society of China*, 2010, **20**, 1550-1554.
16. S. Gu, W. Wang, H. Wang, F. Tan, X. Qiao and J. Chen, *Powder Technol*, 2013, **233**, 91-95.
17. R. L. Penn and J. F. Banfield, *Geochimica et Cosmochimica Acta*, 1999, **63**, 1549-1557.
18. J. F. Banfield, S. A. Welch, H. Zhang, T. T. Ebert and R. L. Penn, *Science*, 2000, **289**, 751-754.
19. R. L. Penn and J. F. Banfield, *Science*, 1998, **281**, 969.
20. X. Cai and A. Zhai, *Rare Metals*, 2010, **29**, 407-412.
21. L. Suber and W. R. Plunkett, *Nanoscale*, 2010, **2**, 128-133.
22. S. R. Forrest and T. A. Witten, *Journal of Physics A: Mathematical and General*, 1979, **12**, L109-L117.
23. T. A. Witten and L. M. Sander, *Phys Rev Lett*, 1981, **47**, 1400-1403.
24. Y. Zhou, S. H. Yu, C. Y. Wang, X. G. Li, Y. R. Zhu and Z. Y. Chen, *Advanced Materials*, 1999, **11**, 850-852.
25. S. Wang and H. Xin, *The Journal of Physical Chemistry B*, 2000, **104**, 5681-5685.
26. T. Qiu, X. L. Wu, Y. F. Mei, P. K. Chu and G. G. Siu, *Applied Physics A*, 2005, **81**, 669-671.

27. X. Wen, Y.-T. Xie, W. C. Mak, K. Y. Cheung, X.-Y. Li, R. Renneberg and S. Yang, *Langmuir*, 2006, **22**, 4836-4842.
28. G. A. Martínez-Castañón, N. Niño-Martínez, J. P. Loyola-Rodríguez, N. Patiño-Marín, J. R. Martínez-Mendoza and F. Ruiz, *Materials Letters*, 2009, **63**, 1266-1268.
29. H. Cölfen and M. Antonietti, *Angewandte Chemie International Edition*, 2005, **44**, 5576-5591.
30. A. Rao and H. Cölfen, in *New Perspectives on Mineral Nucleation and Growth: From Solution Precursors to Solid Materials*, eds. A. E. S. Van Driessche, M. Kellermeier, L. G. Benning and D. Gebauer, Springer International Publishing, Cham, 2017, DOI: 10.1007/978-3-319-45669-0_8, pp. 155-183.
31. J. Fang, B. Ding and X. Song, *Applied Physics Letters*, 2007, **91**, 083108.
32. J. Fang, B. Ding, X. Song and Y. Han, *Applied Physics Letters*, 2008, **92**, 173120.
33. L. Cheng, C. Ma, G. Yang, H. You and J. Fang, *J Mater Chem A*, 2014, **2**, 4534-4542.
34. J. Fang, S. Liu and Z. Li, *Biomaterials*, 2011, **32**, 4877-4884.
35. Z. Yang, l. z, H. You, Z. Li and J. Fang, *Particle-Arrayed Silver Mesocubes Synthesized via Reducing Silver Oxide Mesocrystals for Surface-Enhanced Raman Spectroscopy*, 2014.
36. in *Crystals: Growth, Morphology, & Perfection*, ed. I. Sunagawa, Cambridge University Press, Cambridge, 2005, DOI: DOI: 10.1017/CBO9780511610349.006, pp. 20-59.
37. A. E. Nielsen, *Journal of Crystal Growth*, 1984, **67**, 289-310.
38. T. Yang, Y. Han and J. Li, *Chemical Engineering Science*, 2015, **138**, 457-464.
39. W. Liu, K. Wang, Y. Zhou, X. Guan, P. Che and Y. Han, *CrystEngComm*, 2019, **21**, 1466-1473.
40. J. J. Hoyt and M. Asta, *Physical Review B*, 2002, **65**, 214106.
41. J. Warren, *Nature Materials*, 2006, **5**, 595-596.
42. J. J. Hoyt, M. Asta and A. Karma, *Physical Review Letters*, 2001, **86**, 5530-5533.
43. T. Haxhimali, A. Karma, F. Gonzales and M. Rappaz, *Nature Materials*, 2006, **5**, 660-664.
44. L. Granasy, T. Pusztai, G. Tegze, J. A. Warren and J. F. Douglas, *Phys Rev E*, 2005, **72**.
45. F. Podmaniczky, G. I. Tóth, G. Tegze, T. Pusztai and L. Gránásy, *Journal of Crystal Growth*, 2017, **457**, 24-31.
46. L. Gránásy, L. Rátkai, A. Szállás, B. Korbuly, G. I. Tóth, L. Környei and T. Pusztai, *Metallurgical and Materials Transactions A*, 2014, **45**, 1694-1719.
47. C.-Y. Sun, M. A. Marcus, M. J. Frazier, A. J. Giuffre, T. Mass and P. U. P. A. Gilbert, *ACS Nano*, 2017, **11**, 6612-6622.
48. J. Harris, I. Mey, M. Hajir, M. Mondeshki and S. E. Wolf, *CrystEngComm*, 2015, **17**, 6831-6837.
49. J. P. Andreassen, E. M. Flaten, R. Beck and A. E. Lewis, *Chem Eng Res Des*, 2010, **88**, 1163-1168.
50. A. G. Shtukenberg, Y. O. Punin, E. Gunn and B. Kahr, *Chem Rev*, 2012, **112**, 1805-1838.
51. J.-P. Andreassen, R. Beck and M. Nergaard, *Faraday Discussions*, 2012, **159**, 247-261.
52. Y.-J. Tu, D. Njus and H. B. Schlegel, *Organic & Biomolecular Chemistry*, 2017, **15**, 4417-4431.
53. D. V. Goia, *Journal of Materials Chemistry*, 2004, **14**, 451-458.
54. J. J. De Yoreo and P. G. Vekilov, *Reviews in Mineralogy and Geochemistry*, 2003, **54**, 57-93.
55. R. Liu and A. Sen, *Chemistry of Materials*, 2012, **24**, 48-54.
56. Y. Chen, H. Zhao, Y. Ning, B. Zhao, J. Zheng, T. Yang, M. Liu, F. Yin, S. Li and L. Chen, *RSC Advances*, 2016, **6**, 102528-102533.
57. Z.-Q. Cheng, Z.-W. Li, J.-H. Xu, R. Yao, Z.-L. Li, S. Liang, G.-L. Cheng, Y.-H. Zhou, X. Luo and J. Zhong, *Nanoscale Research Letters*, 2019, **14**, 89.
58. J. Liu, T. Yang, C. Li, J. Dai and Y. Han, *Scientific Reports*, 2015, **5**, 14942.
59. T. Yang and Y. Han, *Crystal Growth & Design*, 2016, **16**, 2850-2859.
60. X. Sun, *Inorganic Materials*, 2010, **46**, 679-682.
61. L. Liu, M. L. Sushko, E. C. Buck, X. Zhang, L. Kovarik, Z. Shen, J. Tao, E. Nakouzi, J. Liu and J. J. De Yoreo, *The Journal of Physical Chemistry Letters*, 2019, DOI: 10.1021/acs.jpclett.9b02110.
62. M. Luty-Błocho, K. Pacławski, M. Wojnicki and K. Fitzner, *Inorganica Chimica Acta*, 2013, **395**, 189-196.
63. H. Bao, T. Bihr, A.-S. Smith and R. N. Klupp Taylor, *Nanoscale*, 2014, **6**, 3954-3966.
64. L. Wang and J.-P. Andreassen, *Chemical Engineering & Technology*, 2014, **37**, 1399-1407.
65. R. Beck and J. P. Andreassen, *J Cryst Growth*, 2010, **312**, 2226-2238.
66. E. G. Ball, *Journal of Biological Chemistry*, 1937, **118**, 219-239.
67. N. Williams and J. Yandell, *Australian Journal of Chemistry*, 1982, **35**, 1133-1144.
68. T. Liu, D. Li, D. Yang and M. Jiang, *Mater Lett*, 2011, **65**, 628-631.
69. C. Dong, X. Zhang, H. Cai, C. Cao, K. Zhou, X. Wang and X. Xiao, *Advanced Powder Technology*, 2016, **27**, 2416-2423.
70. D. Goia and E. Matijević, *Colloids and Surfaces A: Physicochemical and Engineering Aspects*, 1999, **146**, 139-152.
71. E. Matijevic and D. Goia, *Croat Chem Acta*, 2007, **80**, 485-491.
72. B. J. Morrow, E. Matijević and D. V. Goia, *Journal of Colloid and Interface Science*, 2009, **335**, 62-69.
73. Y.-Y. Kim, A. S. Schenk, J. Ihli, A. N. Kulak, N. B. J. Hetherington, C. C. Tang, W. W. Schmahl, E. Griesshaber, G. Hyett and F. C. Meldrum, *Nature Communications*, 2014, **5**, 4341.
74. Y. O. Punin, *Journal of Structural Chemistry*, 1994, **35**, 616-624.